The Astrophysical Journal, 965:57 (11pp), 2024 April 10 https://doi.org/10.3847/1538-4357/ad2705

Measuring the Variance of the Macquart Relation in Redshift–Extragalactic Dispersion Measure Modeling

Jay Baptista[1,2], J. Xavier Prochaska[3,4,5], Alexandra G. Mannings[3], C. W. James[6], R. M. Shannon[7], Stuart D. Ryder[8,9], A. T. Deller[7], Danica R. Scott[6], Marcin Glowacki[6], and Nicolas Tejos[10]
[1] Department of Astronomy and Astrophysics, Yale University, New Haven, CT 06520, USA; jaymarie@stanford.edu
[2] Department of Physics, Stanford University, Stanford, CA 94305, USA
[3] Department of Astronomy and Astrophysics, University of California, Santa Cruz, CA 95064, USA
[4] Kavli Institute for the Physics and Mathematics of the Universe (Kavli IPMU), 5-1-5 Kashiwanoha, Kashiwa, 277-8583, Japan
[5] Division of Science, National Astronomical Observatory of Japan, 2-21-1 Osawa, Mitaka, Tokyo 181-8588, Japan
[6] International Centre for Radio Astronomy Research, Curtin University, Bentley, WA 6102, Australia
[7] Centre for Astrophysics and Supercomputing, Swinburne University of Technology, Hawthorn, VIC 3122, Australia
[8] School of Mathematical and Physical Sciences, Macquarie University, NSW 2109, Australia
[9] Astrophysics and Space Technologies Research Centre, Macquarie University, Sydney, NSW 2109, Australia
[10] Instituto de Física, Pontificia Universidad Católica de Valparaíso, Casilla 4059, Valparaíso, Chile
Received 2023 May 11; revised 2024 January 26; accepted 2024 February 5; published 2024 April 4

Abstract

The Macquart relation describes the correlation between the dispersion measure (DM) of fast radio bursts (FRBs) and the redshift z of their host galaxies. The scatter of the Macquart relation is sensitive to the distribution of baryons in the intergalactic medium including those ejected from galactic halos through feedback processes. The variance of the distribution in DMs from the cosmic web ($\mathrm{DM_{cosmic}}$) is parameterized by a fluctuation parameter F. In this work, we present a new measurement of F using 78 FRBs of which 21 have been localized to host galaxies. Our analysis simultaneously fits for the Hubble constant H_0 and the DM distribution due to the FRB host galaxy. We find that the fluctuation parameter is degenerate with these parameters, most notably H_0, and use a uniform prior on H_0 to measure $\log_{10} F > -0.86$ at the 3σ confidence interval and a new constraint on the Hubble constant $H_0 = 85.3^{+9.4}_{-8.1}$ km s^{-1} Mpc^{-1}. Using a synthetic sample of 100 localized FRBs, the constraint on the fluctuation parameter is improved by a factor of $\sim$2. Comparing our F measurement to simulated predictions from cosmological simulation (IllustrisTNG), we find agreement between redshifts $0.4 < z$ and $z < 2.0$. However, at $z < 0.4$, the simulations underpredict F, which we attribute to the rapidly changing extragalactic DM excess distribution at low redshift.

Unified Astronomy Thesaurus concepts: Radio transient sources (2008); Radio bursts (1339); Cosmological parameters (339); Intergalactic medium (813); Hubble constant (758)

1. Introduction

In galaxy formation models, active galactic nuclei (AGNs) and stellar feedback have provided mechanisms for regulating star formation and evacuating gas out of low-mass halos (Cen & Ostriker 2006; Davé et al. 2011). In simulations without baryonic outflows, galaxies simply produce too many stars and have higher-than-observed star formation rates (Davé et al. 2011). These outflow processes are also critical in understanding how the intergalactic medium (IGM) becomes enriched and how the galaxies and the IGM coevolve.

Not only is understanding the nature of feedback crucial in reproducing realistic galaxy properties in cosmological-baryonic simulations but also in understanding the channels where these "missing" baryons may have left halos and are prevented from reaccretion. Gas accretion onto galaxies from cold gas filaments is exceptionally efficient. Baryonic feedback is a preventative process that not only enriches the IGM but also removes baryons and restricts accretion from the IGM (Kereš et al. 2005). For example, in the SIMBA suite of cosmological hydrodynamic simulations, feedback from AGN jets can cause 80% of baryons in halos to be evacuated by $z = 0$ (Davé et al. 2019; Appleby et al. 2021; Sorini et al. 2022).

A comparison of simulation suites shows that different feedback prescriptions can eject baryons at various distances beyond the halo boundary, feeding gas into the reservoir of diffuse baryons (e.g., Ayromlou et al. 2023). Thus, to constrain the strength of AGN and stellar feedback processes, one must be able to constrain the distribution of baryons in the IGM to discriminate between these feedback models.

Determining the distribution of these ejected baryons is difficult. Emission and absorption lines from baryons in the IGM are extremely difficult to detect due to their high temperatures and low densities (Fukugita et al. 1998; Cen & Ostriker 2006; Shull et al. 2012; McQuinn 2014). However, the advent of fast radio bursts (FRBs) presents a new opportunity to probe the intergalactic distribution of baryons and provide a novel approach to measuring feedback strength (McQuinn 2014; Muñoz & Loeb 2018).

FRBs are sensitive to the line-of-sight free-electron density where the integrated free-electron density yields the dispersion measure (DM) of the signal (Lorimer et al. 2007). A redshift can be estimated if the spatial localization of the FRB overlaps with a galaxy with a known redshift (assuming the FRB progenitor indeed lies within that galaxy; Aggarwal et al. 2021). This FRB redshift-extragalactic DM (z–$\mathrm{DM_{EG}}$) correlation known as the Macquart relation (Macquart et al. 2020) is

sensitive to cosmological properties of the Universe (e.g., James et al. 2022b). By using a sophisticated FRB observational model that can account for observational biases, intergalactic gas distribution, burst width, and DM, it is possible to use FRB surveys to infer the distribution of baryons in the Universe (McQuinn 2014; James et al. 2022b; Lee et al. 2022).

Halos with weaker feedback retain their baryons more effectively, leading to halos with higher $\mathrm{DM_{EG}}$ contributions and voids with lower $\mathrm{DM_{EG}}$ contributions (McQuinn 2014). An FRB can travel either through extremely low DM voids or pass through extremely high DM halos suddenly, leading to enhanced scatter in the z–$\mathrm{DM_{EG}}$ distribution. On the other hand, halos with stronger feedback will cause the z–$\mathrm{DM_{EG}}$ distribution to show less scatter. Feedback processes are able to more effectively relocate halo baryons into the IGM, causing interhalo voids to have higher DM. This leads to a more homogeneous universe.

The goal of this paper is part of a broader effort to constrain prescriptions on galactic feedback as determined by measuring the variance of the Macquart relation using a sample of FRBs. Current methods that are employed to constrain the variance of the z–$\mathrm{DM_{EG}}$ involve stacking analyses and leveraging two-point statistics. Weighted stacking can measure DM excess by binning FRB DM measurements by the halo mass the FRB intercepts; however, it loses efficacy at high redshift ($z > 0.1$; Wu & McQuinn 2023). The latter works by correlating galaxy survey catalogs (binned along redshift) and FRB catalogs (binned along DM; Rafiei-Ravandi et al. 2020). The current limitation of this approach is that it ignores numerous propagation effects (e.g., scattering and plasma lensing) and has yet to explore model assumptions (e.g., free-electron profiles, Rafiei-Ravandi et al. 2020).

This work leverages a complex forward model of the z–$\mathrm{DM_{EG}}$ distribution to measure the variance of the Macquart relation, which is a direct tracer of the intergalactic baryon distribution (if one is able to sufficiently model the DM contributions from the galaxy and the FRB host galaxy). The advantages of the forward model used in this work are that it employs direct redshift measurements of the FRB host galaxies and is capable of measuring the variance out to $z > 0.5$ if the FRB sample permits. This observable also can be synergistically combined with other direct observables of the IGM baryon distribution such as the thermal Sunyaev–Zeldovich effect (Pandey et al. 2023).

This paper is organized as follows: Section 2 outlines the modeling of the z–DM distribution and how the fluctuation parameter F influences observations of the FRB distribution; Section 3.1 presents our measurements on the fluctuation parameter F and the fits on other parameters used in the z–$\mathrm{DM_{EG}}$ model; Section 3.2 details our forecast on F by sampling 100 synthetic FRBs and finding the probability distribution functions of our model parameters based on the synthetic survey; Section 4 discusses our results in the context of constraining cosmic feedback strength and parameter degeneracies and compares our measurements to simulations. We emphasize that this work is a first attempt at demonstrating that the Macquart variance is a measurable observable, acknowledging the presence of some obfuscating factors that may necessitate future adjustments and fitting. It is crucial to underscore that the field of FRB cosmology is emergent, and the usage of this observable quantity will allow future works to compare with simulations or other expectations.

2. Methods

2.1. Basic Formalism

This work makes use of the FRB code ZDM developed by James et al. (2022b) to model observables of FRB populations. The model assumes that the DM measurement of an FRB can be decomposed as $\mathrm{DM_{FRB}} = \mathrm{DM_{ISM}} + \mathrm{DM_{halo}} + \mathrm{DM_{EG}}$, where $\mathrm{DM_{ISM}}$ and $\mathrm{DM_{halo}}$ are the DM contributions due to the Milky Way's interstellar medium (modeled using NE2001; Cordes & Lazio 2002) and diffuse ionized gas in the Galaxy's halo (Prochaska & Zheng 2019; Cook et al. 2023; Ravi et al. 2023). The $\mathrm{DM_{EG}}$ term is the extragalactic DM contribution and is decomposed into $\mathrm{DM_{EG}} = \mathrm{DM_{cosmic}} + \mathrm{DM_{host}}$ where $\mathrm{DM_{cosmic}} = \mathrm{DM_{IGM}} + \mathrm{DM_{halo,\ EG}}$ is the contribution due to baryons in the IGM and intersecting halos in the line of sight, and $\mathrm{DM_{host}}$ is the contribution due to the host galaxy of the FRB signal. The contribution from the host ($\mathrm{DM_{host}}$) is modeled as a log-normal distribution with a width of $\exp(\mu)$ and a logarithmic scatter of σ_{host} where μ and σ_{host} are free parameters of the model.

The width of the z–$\mathrm{DM_{EG}}$ distribution at a fixed redshift is characterized in part by the probability distribution of measuring the $\mathrm{DM_{cosmic}}$ of an FRB above or below $\langle \mathrm{DM_{cosmic}} \rangle$. This distribution is described by $p_{\mathrm{cosmic}}(\Delta)$, where $\Delta \equiv \mathrm{DM_{cosmic}}/\langle \mathrm{DM_{cosmic}} \rangle$:

$$p_{\mathrm{cosmic}}(\Delta) = A\Delta^{-\beta} \exp\left[-\frac{(\Delta^{-\alpha} - C_0)^2}{2\alpha^2 \sigma_{\mathrm{DM}}^2} \right], \tag{1}$$

where $\alpha \simeq 3$ and $\beta \simeq 3$ are the inner and outer slopes of the gas profile density of intervening halos (based on numerical simulations from Macquart et al. 2020), C_0 shifts the distribution such that $\langle \Delta \rangle = 1$, and σ_{DM} represents the spread of the distribution (Macquart et al. 2020).

σ_{DM}^2 is the fractional variance of the non-Gaussian distribution given by Equation (1). It is manifestly unitless and is dependent on the distribution of ionized gas in halos and large-scale structure along the line of sight.

Owing to the approximately Poisson nature of intersecting halos and other structures, one expects $\sigma_{\mathrm{DM}} \propto z^{-1/2}$ (Macquart et al. 2020), and one is motivated to introduce a fluctuation parameter F:

$$\sigma_{\mathrm{DM}}(\Delta) = Fz^{-0.5}. \tag{2}$$

The non-Gaussian probability distribution function is motivated by theoretical treatments of the IGM and galaxy halos as detailed in Macquart et al. (2020). The fractional variance σ_{DM}^2 is expected to decrease with redshift owing to the increase of the number of intersecting halos along the line of sight to and thus lower statistical variation around $\langle \mathrm{DM_{cosmic}} \rangle$. In the limit where σ_{DM} is small, the distribution becomes Gaussian to capture the Gaussianity of large-scale structures. This is physically motivated as halo gas is more diffuse in this limit and thus contributions to the variance due to halo gas are insignificant. In the limit where σ_{DM} is large, the halo gas contribution becomes significant (Macquart et al. 2020).

As the fluctuation parameter increases, i.e., $F \sim 1$, the spread of $\mathrm{DM_{cosmic}}$ increases. Figure 1 shows $p(\mathrm{DM}|z)$ for two extreme values of F and the resultant, substantial changes to the width of the $\mathrm{DM_{EG}}$ distribution at any given redshift.

Table 1
New FRB Detections Detected in 2022 Used in Addition to the FRB Surveys Used in James et al. (2022a)

Name	Survey	DM (pc cm^{-3})	DM_{ISM} (pc cm^{-3})	ν (MHz)	S/N	z
20220725A	CRAFT/ICS 900 MHz	290.4	30.7	920.5	12.7	0.1926
20220501C	CRAFT/ICS 900 MHz	449.5	30.6	863.5	16.1	0.381
20211203C	CRAFT/ICS 900 MHz	636.2	63.4	920.5	14.2	0.34386
20220918A	CRAFT/ICS 1.3 GHz	656.8	40.7	1271.5	26.4	⋯
20220610A	CRAFT/ICS 1.3 GHz	1458.1	31.0	1271.5	29.8	1.016
20220531A	CRAFT/ICS 1.3 GHz	727.0	70.0	1271.5	9.7	⋯
20221106A	CRAFT/ICS 1.6 GHz	344.0	34.8	1631.5	35.1	⋯
20220105A	CRAFT/ICS 1.6 GHz	583.0	22.0	1632.5	9.8	0.2785

Note. The FRB name, S/N-maximizing DM, DM_{ISM} estimated using the NE2001 model of Cordes & Lazio (2002), central frequency of observation ν, measured signal-to-noise ratio S/N, redshift z, and original reference. Where redshifts are not given, this is because (a): no voltage data were dumped, preventing radio localization; (b) optical follow-up observations are not yet complete; (c) substantial Galactic extinction has challenged follow-up optical observations; (d) the host galaxy appears too distant to accurately measure a redshift. All FRBs referenced are from R. Shannon et al. (2023, in preparation) with the exception of FRB20220610A (Ryder et al. 2022).

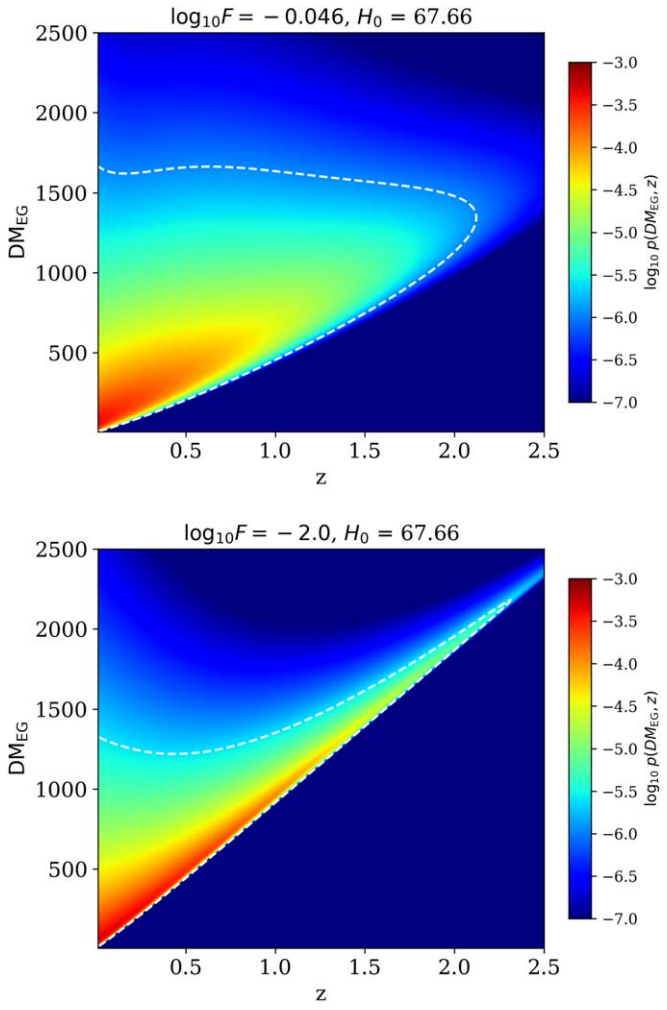

Figure 1. Upper panel: the $p(DM_{EG}|z)$ distribution, which admits a high fluctuation parameter (low galactic feedback efficiency). Lower panel: the $p(DM_{EG}|z)$ distribution, which admits a low fluctuation parameter (high galactic feedback efficiency). The white dashed line indicates the 95th percentile contour. Note that the distribution primarily falls below the mean due to the rare population of high DM FRBs that result from intersections with the host galaxy and/or very massive galaxy halos along the line of sight.

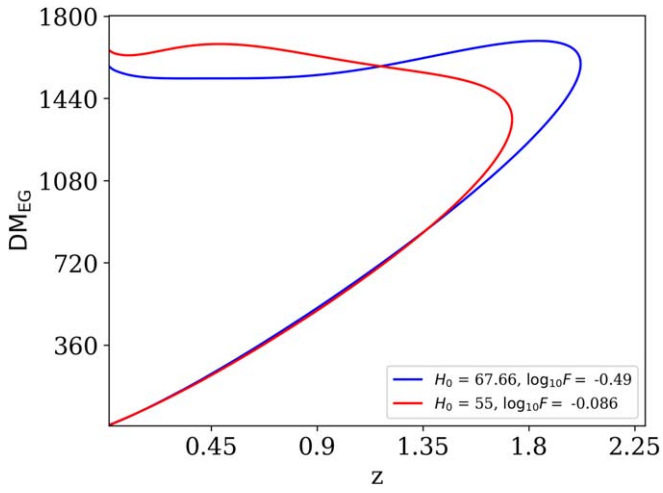

Figure 2. Ninety-fifth percentile contours of two $p(DM_{EG}|z)$ distributions with different prescriptions on the Hubble constant H_0 and the fluctuation parameter F. Note that the lower contours ("the DM cliff") of both models are nearly identical to each other. Since the DM cliff places a stronger constraint on H_0 and F than the upper contour, we expect a high degree of degeneracy between H_0 and F. The units of DM_{EG} are in parsec per cubic centimeter and the units of H_0 are in kilometers per second per megaparsec.

The variance in DM_{EG}, however, is influenced by both σ_{host} and F. However, at high redshift, the contribution to the variance of DM_{EG} due to σ_{host} may decrease relative to the contributions by DM_{cosmic} and, inherently, F. In James et al. (2022a), their work assumes that uncertainties attributed to the fixed value of F can be aggregated into uncertainties in σ_{host}; however, at high redshift, the assumption breaks down as the uncertainty in F becomes larger than the true constraint in σ_{host}.

Although Macquart et al. (2020) restrict their fitting of the fluctuation parameter to $F \in [0.09, 0.32]$ based on semianalytic models, we sample a wide range of $F \in [0, 1]$. We opt for a logarithmic sampling of the fluctuation parameter to efficiently sample this domain: $\log_{10} F \in [-2, 0]$. The choice of uniform sampling over a logarithmic domain is also motivated by F as a scale parameter, and thus this choice of prior is uninformative (i.e., represents an agnostic state of knowledge).

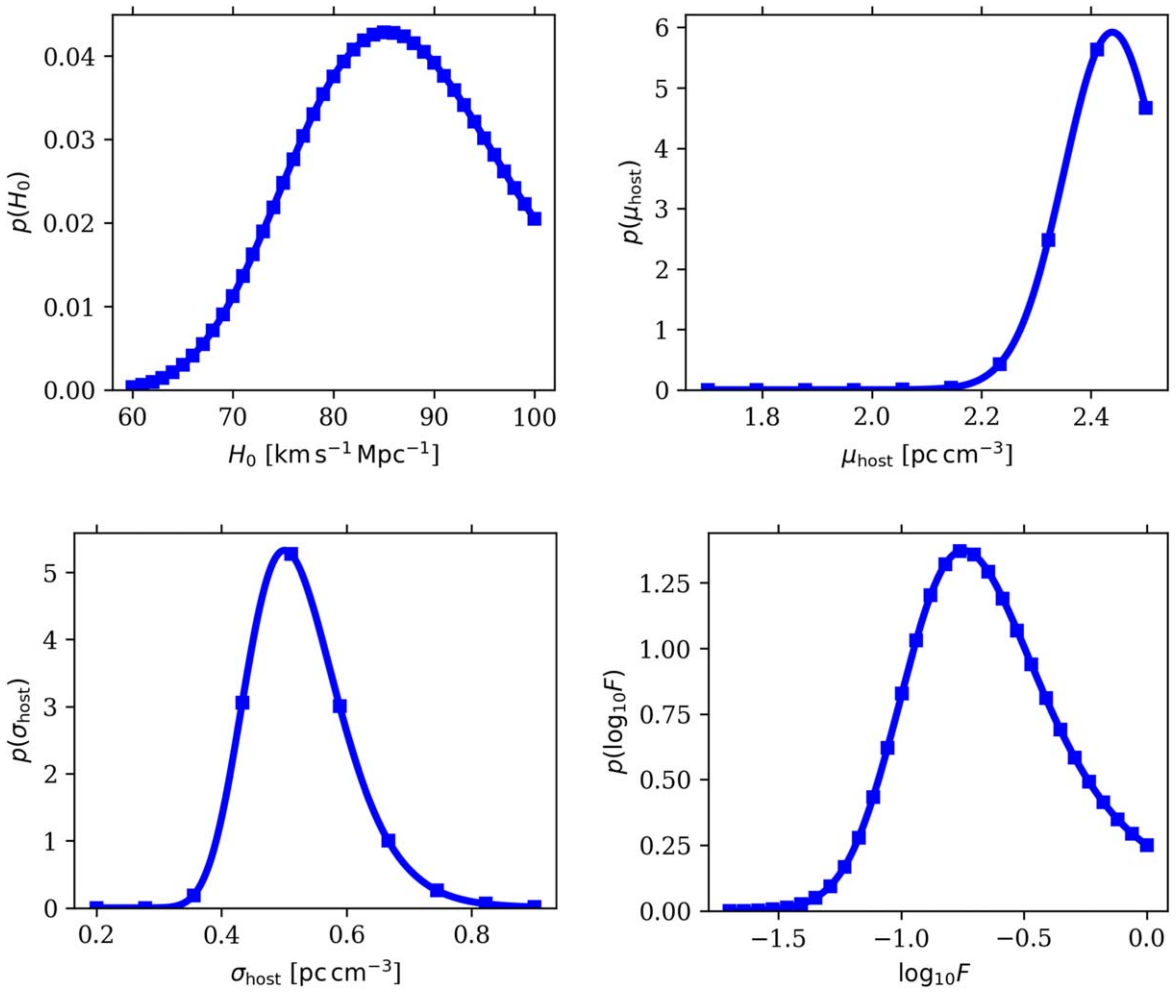

Figure 3. The calculated 1D likelihood functions using 78 FRBs (21 FRBs with redshifts). F is measured to be $\log_{10}F = -0.75^{+0.33}_{-0.25}$ with no priors on H_0. There is a loss of constraining power on H_0 compared to the measurement by James et al. (2022a) when allowing the F parameter to vary.

The additional parameters used in the model include H_0 (acceleration of the Universe's expansion), the $\rm DM_{EG}$ contribution due to the FRB host galaxy, and other parameters that govern the FRB luminosity function and redshift distribution. The model assumes that the $\rm DM_{EG}$ contribution from the FRB host galaxy can be modeled as a log-normal distribution with a mean of $\mu_{\rm host}$ (or $\rm DM_{host}$) and a spread of $\sigma_{\rm host}$.

In terms of the luminosity function, the maximum burst energy is given as $E_{\rm max}$, and the integral slope of the FRB luminosity function is controlled by γ. The volumetric burst rate (Φ) is controlled by the parameter $n_{\rm sfr}$ assuming a star formation rate: $\Phi \propto \rm SFR(z)^{n_{sfr}}$. Additionally, α is the spectral index that sets a frequency-dependent FRB rate as $\Phi(z, \nu) = \Phi(z)\nu^{\alpha}$ (James et al. 2022a).

Table 2
z–DM Grid Parameters

Parameter	Unit	Fiducial	Min.	Max.	N
H_0	km s^{-1} Mpc^{-1}	67.66	60.00	80.00	21
$\log_{10}F$	⋯	−0.49	−1.70	0.00	30
$\mu_{\rm host}$	pc cm^{-3}	2.18	1.70	2.50	10
$\sigma_{\rm host}$	pc cm^{-3}	0.48	0.20	0.90	10
α	⋯	0.65	⋯	⋯	⋯
γ	⋯	−1.01	⋯	⋯	⋯
$n_{\rm sfr}$	⋯	0.73	⋯	⋯	⋯
$\log_{10}E_{\rm max}$	erg	41.40	⋯	⋯	⋯

Note. This table indicates the parameters of the high-resolution grid run. Nondegenerate parameters are held to the fiducial values. N is the number of cells between the minimum and maximum parameter values.

2.2. *Measuring* F *Using FRB Survey Data*

To measure the fluctuation parameter, we perform a simultaneous fit of the parameters in the ZDM model implemented by James et al. (2022a). We obtain the probability distributions of each parameter by a brute-force grid search based on the ranges specified in Table 2 and calculating the likelihoods for each permutation of parameter values.

We fit these parameters using both the FRB sample used in James et al. (2022a) and newly detected or analyzed FRBs (see Table 1), which were collected from the Parkes and ASKAP telescopes. Of this sample of 78 measured FRBs, 57 FRBs do not have measured redshifts. Constraining the redshift of an FRB greatly increases the statistical power, as a single FRB with a redshift can have the same constraining power as roughly 20 FRBs without redshifts (James et al. 2022a). Thus our inclusion of seven new CRAFT/ICS FRBs detected over three frequency ranges (four with host redshifts), and our

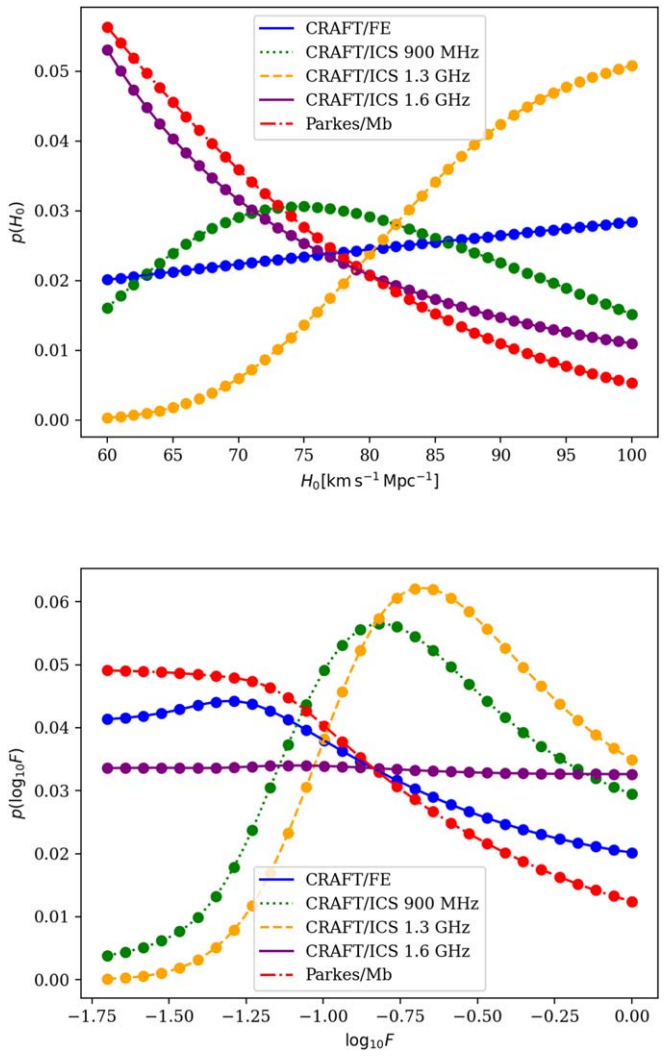

Figure 4. Upper panel: 1D likelihood functions of H_0 based on different FRB surveys used in this work. Compared to the survey contribution constraints (see Figure 7 in James et al. 2022a), the constraining power of each survey is diminished. Lower panel: same as upper panel for likelihood functions of $\log_{10}F$. The CRAFT/ICS 900 MHz and 1.3 GHz surveys provide the most constraining power on F and H_0 as they contain more redshifts than the other surveys.

identification of the host galaxy of FRB20211203C at $z = 0.344$, provides a significant increase in statistical precision.

There is a slight bias in this sample, as we include FRB20220610A, which has an energy exceeding the previously estimated turnover $E_{\rm max}$ by a factor of 3.5–10, depending on the assumed spectral behavior (Ryder et al. 2022). FRB20210912A has a lower DM of 1234.5 pc cm^{-3}, but it does not have an identified redshift, perhaps due to the distance to its host galaxy (L. Marnoch et al. 2024, in preparation). Therefore, the inclusion of some data is redshift-dependent. Given that our sample is statistically limited, we assume the resulting bias to be small compared to the gain in precision.

In contrast to the James et al. (2022a) analysis, we hold model parameters that are not degenerate to their fiducial values. These parameters were determined to be nondegenerate with F running the model using a low-resolution grid search on synthetic data to determine if F correlated with any of the other model parameters. From this preliminary analysis, we fix the following parameters that were found to be nondegenerate with F: α, γ, $E_{\rm max}$, and $n_{\rm sfr}$. On the other hand, we expect the fluctuation parameter to be degenerate with the other model parameters. In particular, we expect the Hubble constant H_0—the cosmological parameter that quantifies the expansion of the universe–to be degenerate with the fluctuation parameter F.

We examine this degeneracy further in Figure 2, which shows the 95th percentile contours for $p({\rm DM}|z)$ for two models with very different F and H_0 values. One notes that the lower contours (${\rm DM_{EG}} \lesssim 720$, $z \lesssim 1.3$) of both realizations look nearly identical. Although the contours differ above the mean, the bulk of the constraining power on F is in the lower contour or "DM cliff." Therefore, we anticipate F and H_0 to be highly correlated.

The distribution at the low DM end of $p({\rm DM_{EG}}|z)$ exhibits a sharp cutoff and provides strong constraints on H_0 since there is a minimum imparted ${\rm DM_{cosmic}}$ from voids and is not impeded by the ${\rm DM_{EG}}$ contributions from large-scale structures like filaments or halos. And while the contours do have modest differences at high z, high ${\rm DM_{EG}}$, these can be difficult to distinguish from host galaxy contributions to ${\rm DM_{EG}}$.

2.3. Forecasting the Fluctuation Parameter F Using Synthetic FRBs

Future radio surveys are expected to widely increase the number of subarcsecond localized FRBs. Thus, the constraining power on F will greatly increase. To explore this scenario, we generate a forecast on the fluctuation parameter by replicating our analysis using a synthetic FRB survey. A sample of 100 localized synthetic FRBs was drawn assuming the distribution of FRBs followed the fiducial z–DM distribution (Table 2). With this synthetic survey, we calculate the associated 4D likelihood matrix and make a forecast on the fluctuation parameter by adopting different priors on H_0.

3. Results

3.1. Parameter Likelihoods from FRB Surveys

In Figure 3, we present the 1D PDFs of each parameter determined from the 78 FRBs collected from the ASKAP and Parkes Radio Telescopes. In comparison to James et al. (2022a), there is a significant loss of constraining power on H_0 by including F as a free parameter. We measure a Hubble constant to be $85.3^{+9.4}_{-8.1}$, which is 1.5 times more uncertain than the H_0 measurement in James et al. (2022a). We attribute the uncertainty to the degeneracy between H_0 and F as indicated by the strong anticorrelation in Figures 2 and 5.

To understand how our survey data at different frequencies contribute to the constraining power on H_0 and F, we replicate the survey contribution determination from James et al. (2022a), which provides the 1D parameter likelihood across different FRB surveys with the Murriyang (Parkes) and Australian Square Kilometre Array (ASKAP). Figure 4 shows the 1D PDFs of H_0 and $\log_{10}F$ across the different surveys used in this analysis. We observe that the CRAFT 1.3 GHz and 900 MHz surveys tend to have stronger constraining power as they contain more FRBs with measured distances (10 and 7 redshifts respectively) than the rest of the surveys.

In Figure 5, we present the 2D likelihoods of each parameter against F. We observe correlations between F and the FRB host galaxy parameters ($\mu_{\rm host}$, $\sigma_{\rm host}$), which we expect to be degenerate given that they both influence the variance of $\langle {\rm DM}_{\rm cosmic} \rangle$. As expected from Figure 2, the degeneracy in the lower bound (or cliff) of the z–${\rm DM}_{\rm EG}$ distribution results in the strong anticorrelation of H_0 and F, resulting in a loss of constraining power on H_0 when allowing F to vary. A corner plot of the various model parameters is presented in Figure 6.

Our initial simultaneous fit does not implement any priors on the model parameters. As motivated by the H_0–F degeneracy in Figure 2, we determine the 1D likelihoods of $\log_{10} F$ by limiting our grid to different values of H_0. When we consider a uniform prior on H_0 between 67.4 and 73.04 km s^{-1} Mpc^{-1} the lower bound is motivated by the H_0 constraint from Planck Collaboration et al. (2020), and the upper bound is motivated by cosmological constraints using Type Ia supernovae (SNe) from Riess et al. (2022).

In Figure 7, we present the 1D likelihood of the fluctuation parameter assuming different priors on H_0. Assuming a uniform prior between the cosmic microwave background (CMB) and SNe-derived values of H_0, we measure the fluctuation parameter to be $\log_{10} F = -0.48^{+0.26}_{-0.18}$ within 1σ ($\log_{10} F = -0.86$ with 99.7% confidence). We present all measurements of the F parameter with different priors on H_0 in Table 3.

3.2. Parameter Likelihoods from Synthetic Surveys

We use a synthetic sample of 100 localized CRACO FRBs to investigate the improvement in constraining power on both F and H_0. In Figure 8, we present the PDFs of each parameter in the grid. We observe that the constraint on H_0 has significantly improved by a factor of 1.7 and is more Gaussian than the previous run with $69.2^{+5.5}_{-4.9}$. Assuming a survey of 100 localized FRBs, the best measurement we can make on H_0 if we adopt a Gaussian prior on $\log_{10} F$ (assuming 1σ corresponds to a 20% error in the measurement) is $67.6^{+3.5}_{-3.4}$ km s^{-1} Mpc^{-1} (see Table 4).

In Figure 9 we show posterior estimates for $\log_{10} F$ using different priors (see Table 3). Using the uniform prior, we obtain a forecast on the fluctuation parameter of $\log_{10} F = -0.60^{+0.19}_{-0.18}$ within 2σ. We note that when compared to Figure 3, there is a definitive upper limit on the fluctuation parameter rather than only a lower limit. Incorporating the uniform prior enhances the constraint on F by a factor of $\sim$1.5, and fixing the value of H_0 can increase the constraint by a factor of 2.5.

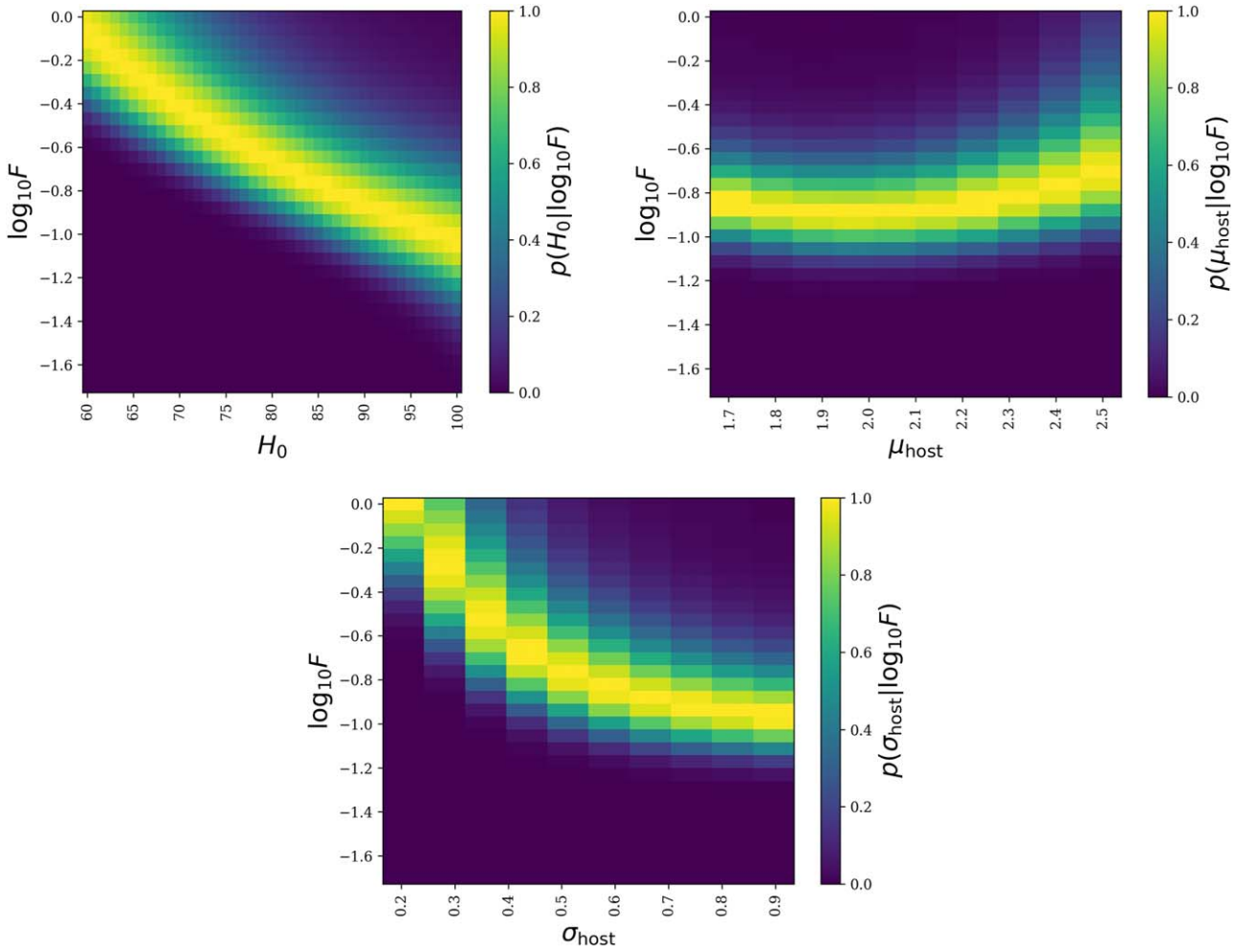

Figure 5. The 2D likelihood functions for each parameter compared against $\log_{10} F$ derived from 78 FRBs (21 FRBs with redshifts). There is a strong anticorrelation between F and H_0. Additionally, we observe strong correlations between F and the host galaxy ${\rm DM}_{\rm EG}$ contribution ($\mu_{\rm host}$, $\sigma_{\rm host}$).

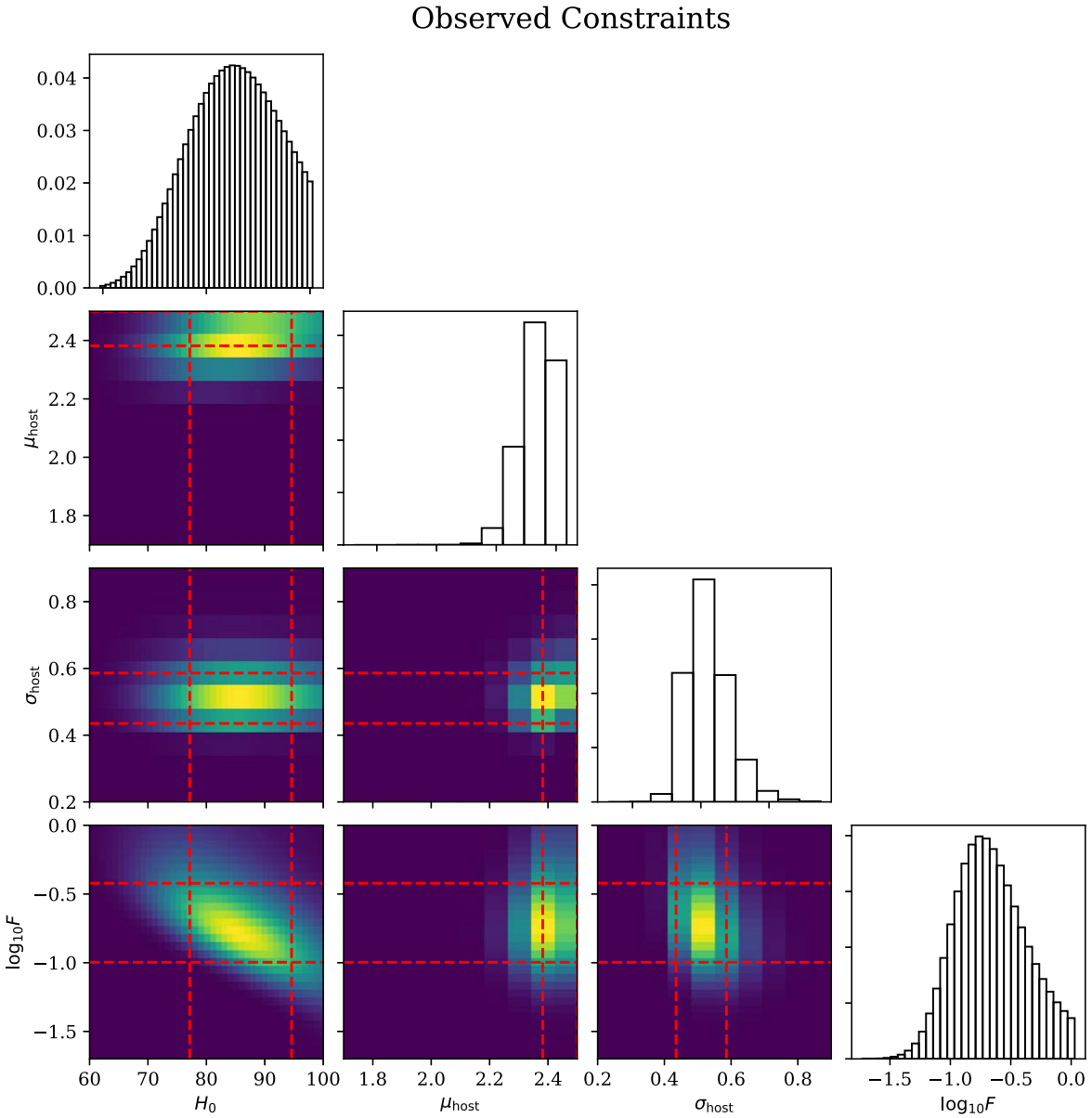

Figure 6. Corner plot of the model parameters fit from 78 FRBs (21 FRBs with redshifts). The red dashed lines indicate the 1σ confidence intervals.

Table 3
Measurements of $\log_{10}F$

Survey	No Prior	Uniform H_0 Prior	CMB H_0	SNe H_0
Observed	$-0.75^{+0.33}_{-0.25}$	$-0.48^{+0.26}_{-0.18}$	$-0.48^{+0.26}_{-0.18}$	$-0.48^{+0.26}_{-0.18}$
Synthetic	$-0.57^{+0.15}_{-0.16}$	$-0.60^{+0.09}_{-0.1}$	$-0.60^{+0.09}_{-0.1}$	$-0.48^{+0.26}_{-0.18}$

Note. This table lists the measurements of the F parameter from the observational FRB survey (78 localized FRBs with 21 redshifts) and the synthetic CRACO survey (100 localized FRBs, all with redshifts). The measurements are presented without a prior, a uniform prior between the CMB ($H_0 = 67.0$ km s^{-1} Mpc^{-1}) and SNe ($H_0 = 73.0$ km s^{-1} Mpc^{-1}) with their respective Gaussian errors on each side, and fixing H_0 to the CMB or SNe estimates.

Table 4
Measurements of H_0

Survey	No Prior	Gaussian Prior
Observed	$85.3^{+9.4}_{-8.1}$	...
Synthetic	$69.2^{+5.5}_{-4.9}$	$67.6^{+3.5}_{-3.4}$

Note. This table lists the measurements of H_0 from the observational FRB survey (78 localized FRBs with 21 redshifts) and the synthetic CRACO survey (100 localized FRBs, all with redshifts). The measurements are presented without a prior on F and a Gaussian prior on F centered at $\log_{10}F \simeq -0.49$ with $\sigma \simeq 0.1$ (20% error on F).

4. Discussion

4.1. Measurement of the Fluctuation Parameter

Our principal result from the population analysis of 78 FRBs (21 with redshifts) is a lower limit on F, which is $\log_{10}F = -0.48^{+0.26}_{-0.18}$ (-0.86 at 99.7% confidence). This measurement is motivated by James et al. (2022a), where they noted that for future localization of FRBs beyond $z \gtrsim 1$, F may need to be fitted explicitly. We note that this observation is only made when adopting a prior between the CMB and SNe values of H_0.

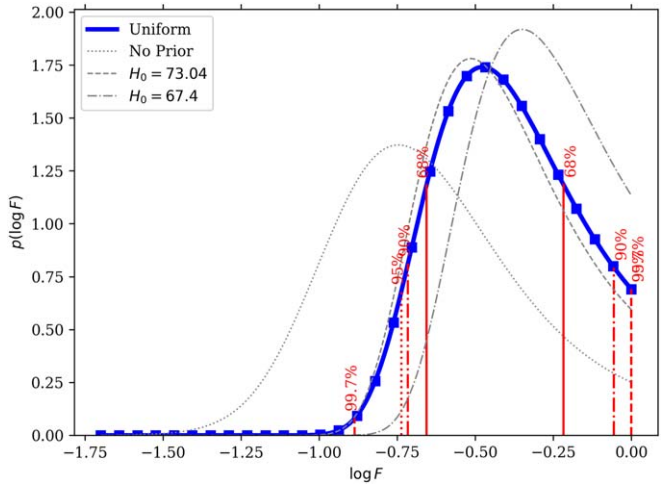

Figure 7. 1D survey likelihoods of $\log_{10} F$ assuming different priors on H_0. The dotted gray line is the original 1D likelihood without any priors on H_0. The blue line is the likelihood that adopts a uniform prior on $H_0 \in [67.4, 73.04]$. The dashed gray line is the likelihood adopting $H_0 = 67.0$ km s^{-1} Mpc^{-1}. The dashed–dotted gray line is the likelihood adopting $H_0 = 73.0$ km s^{-1} Mpc^{-1}. Adopting a prior on H_0 or fixing the values of H_0 greatly improves the constraint on F.

4.2. Fluctuation Parameter Degeneracies

Our findings indicate a strong degeneracy between the Hubble constant H_0 and the fluctuation parameter F when simultaneously fitting both within the z–DM modeling framework adopted by James et al. (2022b) that uses $F = 0.32$, which falls within the accepted range of our measurement.

Aside from the degeneracy between F and H_0, we would like to call attention to the possible degeneracy between F and σ_8—the rms amplitude of the matter density field when smoothed with an 8 h^{-1} Mpc filter. In the case of weak feedback ($F \to 1$), more mass would be concentrated within cosmic filaments, increasing the variance of a fixed-mass filter (i.e., σ_8). We expect these two parameters to be inversely coupled. A preliminary analysis varying σ_8 in the CAMELS IllustrisTNG cosmological simulations does show a positive correlation between F and σ_8 (Medlock et al. 2024).

4.3. Forecasting Enhanced Constraints on F

Using a sample of 100 synthetic FRBs (see Figure 9), we are able to constrain both upper and lower limits on the fluctuation parameter out to 3σ. Since we are only able to effectively constrain a lower limit on F, we compare the lower-sided half-maximum widths. We find the left-sided half-maximum width of the synthetic distribution is *half* the width of the current measured distribution. We expect this constraint to only improve with more localizations, which will be easily facilitated with next-generation all-sky radio observatories.

Additionally, it is of interest to see how this method compares to other ways of measuring the baryon distribution in the IGM. For example, an alternative method to constrain AGN and stellar feedback focuses on small-scale deviations in the matter power spectrum (van Daalen et al. 2020). As baryonic feedback significantly influences the mass distribution at smaller scales (higher k), probes of the gas density at those scales (thermal Sunyaev–Zel'dovich effect) can measure the intergalactic baryon distribution (Pandey et al. 2023).

4.4. Comparing with Fluctuation Parameter in IllustrisTNG

Our observed measurement of the fluctuation parameter can also be used to discriminate subgrid physics models in galaxy simulations. Manifestly, the strength of subgrid feedback influences the IGM baryon distribution as galaxies can expel gas into the IGM and impede gas accretion onto the galaxy (Kelly et al. 2022). The measurement of $\langle \mathrm{DM}_{\mathrm{cosmic}} \rangle$ (i.e., F) is sensitive to this process.

In a work by Zhang et al. (2021) to highlight the utility of FRBs in probing the IGM, they generated thousands of FRB sight lines in IllustrisTNG and fitted the observed extragalactic DM excess $p_{\mathrm{cosmic}}(\Delta)$. They provide the fitted parameters as well as the dispersion in the z–$\mathrm{DM}_{\mathrm{EG}}$ distribution σ_{DM}. We convert these values into the fluctuation parameter F by assuming $\sigma_{\mathrm{DM}} = Fz^{-0.5}$.

In Figure 10, we present these derived $\log_{10} F$ values as a function of redshift compared to our measured values. Between $0.4 < z < 2$, our measurements are in fine agreement. However, we observe that the fluctuation parameter in IllustrisTNG appears to be higher at $z \lesssim 0.4$ and lower when $z > 2$.

From the redshift-dependent $\mathrm{DM}_{\mathrm{IGM}}$ distributions derived from IllustrisTNG (Figure 2 from Zhang et al. 2021), distributions between $0.1 < z < 0.4$ are wider, and the modes of each distribution are spread farther apart. This may explain why the IllustrisTNG fluctuation parameter is higher than our measurement as the $\mathrm{DM}_{\mathrm{IGM}}$ distribution functions have larger variance at those redshifts.

To make a proper comparison between our work and Zhang et al. (2021), it may be necessary to introduce a free parameter for the redshift evolution of σ_{DM} instead of simply fixing the redshift exponent to $-1/2$ (Equation (2)).

In addition to how feedback distributes gas into the IGM as measured by F, $\mathrm{DM}_{\mathrm{host}}$ may be measured complementary to F as these prescriptions directly influence the gas properties *within* the host galaxy (Kelly et al. 2022; Mo et al. 2023). Ultimately, this will change the distribution of $\mathrm{DM}_{\mathrm{host}}$ between simulations with different prescriptions as the amplitude and concentration of $\mathrm{DM}_{\mathrm{host}}$ as a function of impact parameter will depend on how a simulated galaxy expels and redistributes gas (Kelly et al. 2022). In the context of Figure 10, Zhang et al. (2020) find that a log-normal distribution can accurately describe $\mathrm{DM}_{\mathrm{host}}$ in IllustrisTNG galaxies, which is in agreement with our forward model ansatz. Since our forward model independently fits $\mathrm{DM}_{\mathrm{host}}$ and F, our analysis can be sensitive to the subgrid treatments of the baryon cycle within a galaxy and the IGM.

5. Conclusions

In this work, we have implemented variance in $\mathrm{DM}_{\mathrm{cosmic}}$ as a free parameter in a forward model of the z–$\mathrm{DM}_{\mathrm{EG}}$ distribution of FRBs. With this adapted model and a survey of 78 ASKAP and Parkes FRBs, we constrain a value for the fluctuation parameter, explore degeneracies within the model, and generate a forecast of the constraint on the fluctuation parameter with a synthetic survey of 100 localized FRBs. The conclusions we draw from this analysis are:

1. Incorporating survey data of 78 (21 with redshifts) FRBs yields a firm lower limit on F. We place the lower limit on F as measured by the survey sample to be $\log_{10} F > -0.89$ at 99.7% confidence. The 900 MHz and 1.3 GHz surveys dominate this constraint due to their

higher number of localizations to host galaxies and their associated redshifts.
2. Forward modeling the FRB data from Parkes and ASKAP, the fluctuation parameter is degenerate with the Hubble constant H_0.
3. We forecast that 100 localized FRBs are sufficient to constrain both an upper and lower limit on the fluctuation parameter. With the greater count of localizations, the half-maximum width of the distribution decreases by ≈50%.
4. Extrapolation of the fluctuation parameter from IllustrisTNG shows agreement between $0.4 < z < 2.0$. Zhang et al. (2021) measure a higher fluctuation parameter at low redshift ($z < 0.4$) and a lower fluctuation parameter beyond $z > 2$. The former result is likely to be an effect of the rapidly evolving $\mathrm{DM_{IGM}}$ distribution at low redshift.

Next-generation radio observatories will significantly improve the constraint on the fluctuation parameter. For example, the Deep Synoptic Array 2000 (DSA-2000) is expected to localize on the order of 10,000 FRBs each year —enough FRBs to sufficiently characterize the baryonic contents of the IGM (Hallinan et al. 2019; Ravi et al. 2019).

Additionally, the FRB Line-of-sight Ionization Measurement From Lightcone AAOmega Mapping (FLIMFLAM) survey is an upcoming spectroscopic survey that seeks to map the intervening cosmic structures and diffuse cosmic baryons in front of localized FRBs (Lee et al. 2022). These FRB foreground data taken in the Southern Hemisphere will be used in conjunction with ASKAP FRB measurements to improve the constraints on the intergalactic baryon distribution (Lee et al. 2022).

These expansions in FRB surveys with localizations are expected to greatly improve the constraints on the fluctuation parameter. With these improved constraints on F, one may leverage this novel observable for investigating feedback and cosmological prescriptions in simulations.

Combining the F parameter with other observables like the thermal Sunyaev–Zeldovich effect that trace the intergalactic baryon distribution, there is ample opportunity to better inform subgrid feedback models (Muñoz & Loeb 2018; Pandey et al. 2023).

This paper constitutes an initial effort at quantifying the variance of the Macquart relation. Though the field of FRB cosmology is in its nascency, we anticipate this novel observable may further motivate comparisons of FRB observations to cosmological simulations and predictions.

Acknowledgments

J.B. acknowledges support from the University of California Santa Cruz under the Lamat REU program, funded by NSF grant AST-1852393, and the Yale Science Technology and Research Scholars Fellowship funded by the Yale College Dean's Office. Authors A.G.M. and J.X.P., as members of the Fast and Fortunate for FRB Follow-up team, acknowledge support from NSF grants AST-1911140, AST-1910471, and AST-2206490. The authors acknowledge the use of the Nautilus cloud computing system which is supported by the following US National Science Foundation (NSF) awards: CNS-1456638, CNS-1730158, CNS-2100237, CNS-2120019, ACI-1540112, ACI-1541349, OAC-1826967, OAC-2112167.

C.W.J. and M.G. acknowledge support by the Australian Government through the Australian Research Council's Discovery Projects funding scheme (project DP210102103).

R.M.S. and A.T.D. acknowledge support through Australian Research Council Future Fellowship FT190100155 and Discovery Project DP220102305.

The Australian SKA Pathfinder is part of the Australia Telescope National Facility (https://ror.org/05qajvd42) which is managed by CSIRO. Operation of ASKAP is funded by the Australian Government with support from the National Collaborative Research Infrastructure Strategy. ASKAP uses the resources of the Pawsey Supercomputing Centre. Establishment of ASKAP, the Murchison Radio-astronomy Observatory and the Pawsey Supercomputing Centre are initiatives of the Australian Government, with support from the Government of Western Australia and the Science and Industry Endowment Fund. We acknowledge the Wajarri Yamatji people as the traditional owners of the Observatory site.

This research is based on observations collected at the European Southern Observatory under ESO programmes 105.204W.003, 105.204W.004, 108.21ZF.001, 108.21ZF.002, 108.21ZF.005, 108.21ZF.006, and 108.21ZF.009.

Appendix

Table 5 presents all best-fit parameters of the model across the observational and synthetic surveys.

Table 5
Best Fit of Model Parameters

Survey	$\log_{10} F$	H_0	μ_{host}	σ_{host}
Observed	$-0.75^{+0.33}_{-0.25}$	$85.3^{+9.4}_{-8.1}$	$2.44^{+0.06}_{-0.06}$	$0.50^{+0.08}_{-0.06}$
Synthetic	$-0.57^{+0.15}_{-0.16}$	$69.2^{+5.5}_{-4.9}$	$2.20^{+0.08}_{-0.09}$	$0.52^{+0.09}_{-0.07}$

Note. This table lists the best-fit model parameters from the observational FRB survey (78 localized FRBs with 21 redshifts) and the synthetic CRACO survey (100 localized FRBs, all with redshifts). The measurements are presented without a prior.

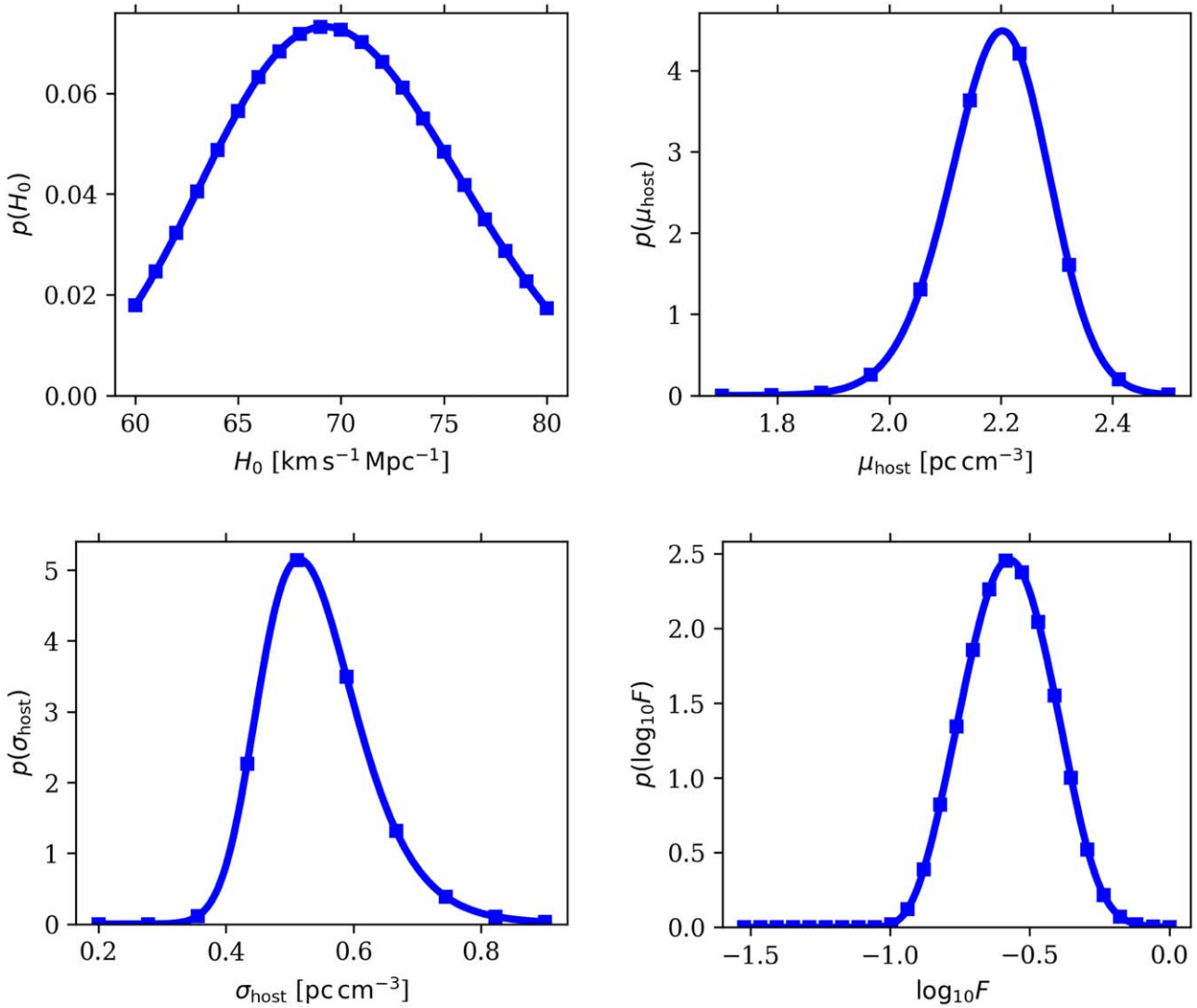

Figure 8. The 1D likelihood functions for each parameter using 100 synthetic FRBs. The constraint on F is enhanced as the uncertainty due to sample size is reduced. Similarly, the constraint on H_0 is improved compared to the observational fit with only 21 redshifts.

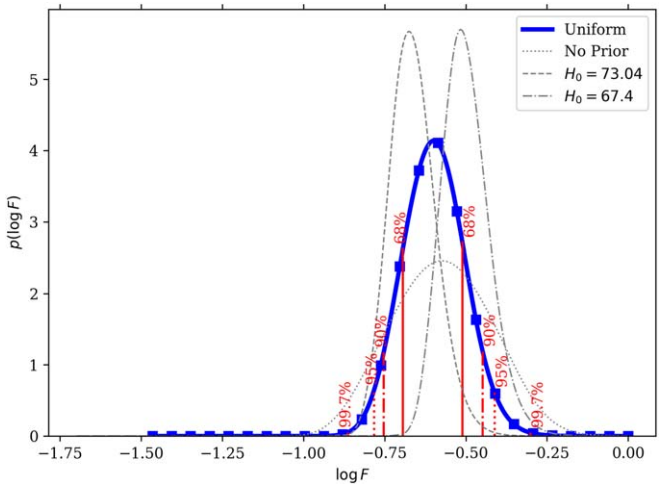

Figure 9. Same as Figure 7 but based on fits to the synthetic FRB sample. Assuming a uniform prior between CMB and SNe values of H_0 equipped with their associated Gaussian errors on both sides, we find $\log_{10}F = -0.60^{+0.09}_{-0.1}$. Fixing the value of H_0 also greatly enhances the constraint on F by a factor of >1.5.

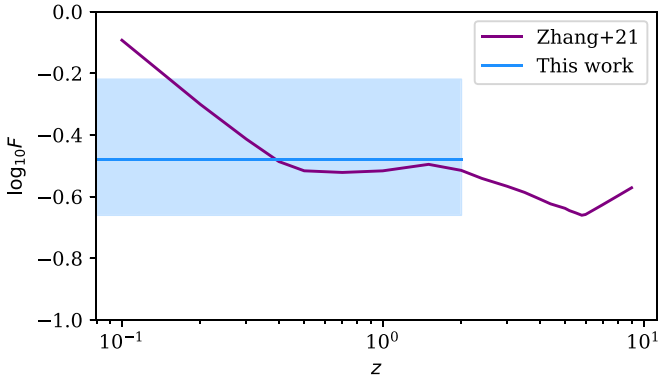

Figure 10. Fluctuation parameters derived from this work, the fiducial value from James et al. (2022a), and the IllustrisTNG values from Zhang et al. (2021). Our measurement on F agrees with the simulated F parameter between the redshifts of $0.4 < z < 2$.

ORCID iDs

Jay Baptista https://orcid.org/0000-0002-9306-1704
J. Xavier Prochaska https://orcid.org/0000-0002-7738-6875
C. W. James https://orcid.org/0000-0002-6437-6176
R. M. Shannon https://orcid.org/0000-0002-7285-6348
Stuart D. Ryder https://orcid.org/0000-0003-4501-8100

References

Aggarwal, K., Budavári, T., Deller, A. T., et al. 2021, ApJ, 911, 95
Appleby, S., Davé, R., Sorini, D., Storey-Fisher, K., & Smith, B. 2021, MNRAS, 507, 2383
Ayromlou, M., Kauffmann, G., Anand, A., & White, S. D. M. 2023, MNRAS, 519, 1913
Cen, R., & Ostriker, J. P. 2006, ApJ, 650, 560
Cook, A. M., Bhardwaj, M., Gaensler, B. M., et al. 2023, ApJ, 946, 58
Cordes, J. M., & Lazio, T. J. W. 2002, arXiv:astro-ph/0207156
Davé, R., Anglés-Alcázar, D., Narayanan, D., et al. 2019, MNRAS, 486, 2827
Davé, R., Oppenheimer, B. D., & Finlator, K. 2011, MNRAS, 415, 11
Fukugita, M., Hogan, C. J., & Peebles, P. J. E. 1998, ApJ, 503, 518
Hallinan, G., Ravi, V., Weinreb, S., et al. 2019, BAAS, 51, 255
James, C. W., Ghosh, E. M., Prochaska, J. X., et al. 2022a, MNRAS, 516, 4862
James, C. W., Prochaska, J. X., Macquart, J. P., et al. 2022b, MNRAS, 509, 4775
Kelly, A. J., Jenkins, A., Deason, A., et al. 2022, MNRAS, 514, 3113
Kereš, D., Katz, N., Weinberg, D. H., & Davé, R. 2005, MNRAS, 363, 2
Lee, K.-G., Ata, M., Khrykin, I. S., et al. 2022, ApJ, 928, 9
Lorimer, D. R., Bailes, M., McLaughlin, M. A., Narkevic, D. J., & Crawford, F. 2007, Sci, 318, 777
Macquart, J. P., Prochaska, J. X., McQuinn, M., et al. 2020, Natur, 581, 391
McQuinn, M. 2014, ApJL, 780, L33
Medlock, I., Nagai, D., Singh, P., et al. 2024, arXiv:2403.02313
Mo, J.-F., Zhu, W., Wang, Y., Tang, L., & Feng, L.-L. 2023, MNRAS, 518, 539
Muñoz, J. B., & Loeb, A. 2018, PhRvD, 98, 103518
Pandey, S., Lehman, K., Baxter, E. J., et al. 2023, MNRAS, 525, 1779
Planck Collaboration, Aghanim, N., Akrami, Y., et al. 2020, A&A, 641, A6
Prochaska, J. X., & Zheng, Y. 2019, MNRAS, 485, 648
Rafiei-Ravandi, M., Smith, K. M., & Masui, K. W. 2020, PhRvD, 102, 023528
Ravi, V., Battaglia, N., Burke-Spolaor, S., et al. 2019, BAAS, 51, 420
Ravi, V., Catha, M., Chen, G., et al. 2023, arXiv:2301.01000
Riess, A. G., Yuan, W., Macri, L. M., et al. 2022, ApJL, 934, L7
Ryder, S. D., Bannister, K. W., Bhandari, S., et al. 2023, Sci, 382, 294
Shull, J. M., Smith, B. D., & Danforth, C. W. 2012, ApJ, 759, 23
Sorini, D., Davé, R., Cui, W., & Appleby, S. 2022, MNRAS, 516, 883
van Daalen, M. P., McCarthy, I. G., & Schaye, J. 2020, MNRAS, 491, 2424
Wu, X., & McQuinn, M. 2023, ApJ, 945, 87
Zhang, G. Q., Yu, H., He, J. H., & Wang, F. Y. 2020, ApJ, 900, 170
Zhang, Z. J., Yan, K., Li, C. M., Zhang, G. Q., & Wang, F. Y. 2021, ApJ, 906, 49